

Ligand Design for Catalytic Dehydrogenation of Formic Acid to Produce High-pressure Hydrogen Gas under Base-free Conditions

Hajime Kawanami,* Masayuki Iguchi, and Yuichiro Himeda

Cite This: <https://dx.doi.org/10.1021/acs.inorgchem.9b01624>

Read Online

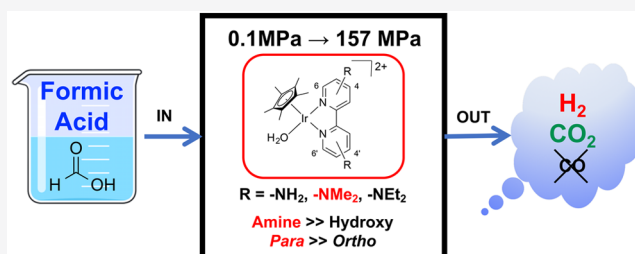
ACCESS |

Metrics & More

Article Recommendations

Supporting Information

ABSTRACT: A series of Cp*Ir (Cp* = pentamethylcyclopentadienyl anion) complexes with amino-functionalized ligands were developed for the production of high-pressure H₂ via catalytic dehydrogenation of formic acid (DFA) in water under base-free conditions. The Ir complexes with 2,2'-bipyridine (bpy) ligands bearing amino or alkylamino groups at the *para* positions exhibited high activity and stability for DFA compared with complexes containing bpy ligands bearing *para*-hydroxyl groups. In addition, *para*-amino groups afforded superior catalytic stability under high-pressure conditions compared with *ortho*-amino groups. By exploiting these amino-functionalized Cp*Ir complexes, it was possible to continuously produce high-pressure CO-free H₂ via selective DFA in water upon the addition of concentrated FA (>99.5 wt %) to the base-free solution. Systematic investigation of the ligand effects on DFA revealed that the presence of alkylamino groups on the bpy ligand enhanced the catalytic activity (initial turnover frequency, TOF), although the stability decreased with increasing alkyl chain length on the amino groups. According to a Hammett plot, the increased catalytic activity of the Ir complexes after the introduction of amino-functionalized ligands may be attributable to the electron-donating effect of *para*-amino groups on the bpy ligand. Based on the experimental results, a reaction mechanism is proposed that involves a hydride intermediate whose stability is affected by the position of the amino groups on the bpy ligand, as confirmed through NMR studies.



INTRODUCTION

Molecular hydrogen (H₂) has attracted considerable attention as an alternative energy source for both direct combustion and use in fuel cells owing to its unique advantages, such as a high energy density by weight (highest among fuels) and the emission of only water vapor upon combustion or electrochemical oxidation, which are beneficial for environmental and energy security.^{1–3} However, the gaseous nature of H₂ limits its volumetric energy density and leads to huge challenges with storage and transportation. Thus, the use of high-pressure H₂ is one solution for increasing the energy density, although the compression process requires a substantial amount of energy, which can be as much as 10–20% of the energy content of the H₂.^{4,5} To circumvent these difficulties, the current state of the art method is to use liquid organic hydrogen carriers (LOHCs), which offer high volumetric hydrogen storage capacities and permit safe and efficient long-term storage and transportation predominantly using the existing infrastructure.³ Among LOHCs, formic acid (FA; HCO₂H), a common bulk chemical that exists as a stable liquid under ambient conditions and can be produced by various industrial processes (reaction between methanol and CO, degradation of biomass, etc.),^{6–11} has been extensively studied for the generation of H₂. In addition, hydrogenation of CO₂ also produces FA, and this interconversion between CO₂ and HCO₂H is considered a

carbon-neutral and environmentally benign system for H₂ production.^{10,12–18}

Hydrogen production via the dehydrogenation of FA (DFA; HCO₂H → H₂ + CO₂) is hindered by a competitive dehydration reaction (HCO₂H → H₂O + CO) that hampers the catalytic activity owing to the formation of CO.¹⁹ For instance, the application of FA as a H₂ generator in proton-exchange membrane (PEM) fuel cells requires highly selective DFA to minimize the production of CO, which rapidly poisons electrocatalysts. Furthermore, CO₂ is also formed from FA alongside H₂, necessitating a separation step for subsequent application of the produced H₂ in fuel cells as well as the recovery of CO₂ as a starting material to complete the CO₂–HCO₂H cycle.²⁰ After obtaining high-pressure gas via DFA, effective H₂/CO₂ separation has been demonstrated using the phase change phenomenon from the supercritical fluid phase to the gas–liquid or gas–solid phase.^{21,22} The pressurization of FA and subsequent reaction to generate high-pressure H₂ avoids the consumption of the large amount of energy required to compress H₂ and reduces the equipment size.

Received: June 1, 2019

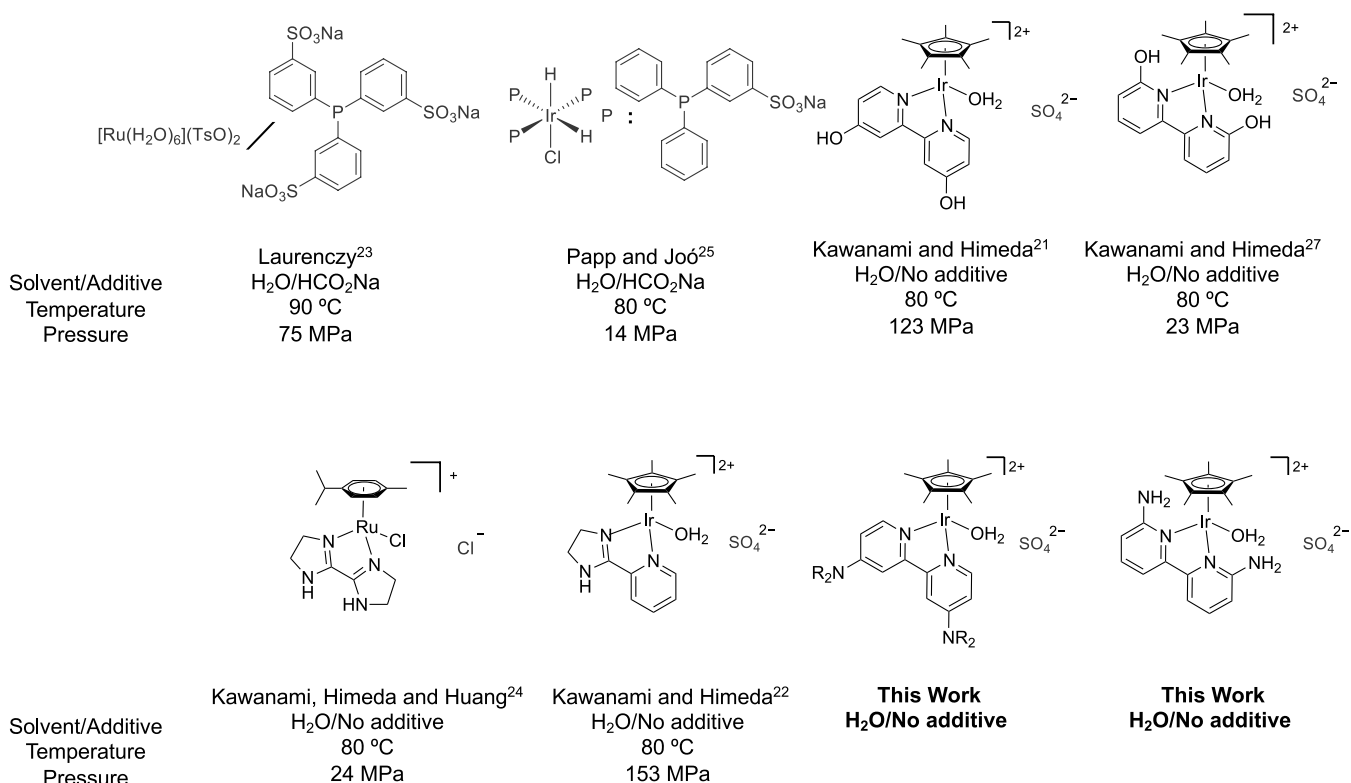


Figure 1. Available literature for high-pressure H₂ production from FA using homogeneous catalysts at mild temperatures ($p \geq 10$ MPa, $T < 100$ °C).

Despite the several distinct advantages of high-pressure DFA over atmospheric-pressure processes, few studies involving mild temperatures have been reported (Figure 1)^{21–26} owing to the comparatively low activity and rapid deactivation of catalysts under high-pressure conditions.²⁷ In addition, the DFA rate was also reported to decrease with increasing generated gas pressures, especially above 10 MPa.²⁸ Addition of a base improved the DFA rate but reduced the FA conversion as well as the generated gas pressure.^{27,29} Therefore, for the high-pressure H₂ production from FA in the absence of a base, the development of a highly active and selective catalyst that retains its stability and durability under acidic conditions at high FA concentrations and high H₂ and CO₂ pressures remains a major challenge.

We have developed a series of Cp^{*}Ir^{III} (Cp^{*} = pentamethylcyclopentadienyl anion) complexes with *N,N'*-bidentate ligands for performing DFA in water at mild temperatures.^{12,13,30–36} The ligand was found to exert a distinct influence on the catalytic activity in terms of turnover frequency (TOF), which increased with increasing electron-donating ability from the ligand to the Ir center of the Cp^{*}Ir complexes.^{12,31,33,35} Interestingly, the presence of a hydroxyl group in the ligand present near the metal center (e.g., the *ortho* positions of 2,2'-bipyridine (bpy)) increased the catalytic activity (= TOF) owing to electronic effects and a proton relay with water (pendent base effect).^{31,37} In our previous work, we observed that an Ir complex containing *para*-hydroxyl groups on the bpy ligand mediated DFA at high pressures with high activity (= TOF) and durability (= TON), whereas rapid deactivation occurred in the case of *ortho*-hydroxyl groups owing to the formation of an Ir trihydride complex.²⁷ Recently, we also reported that it is possible to produce high-pressure H₂ and CO₂ gases above 100 MPa at 80 °C using an Ir complex

containing an aromatic *N,N'*-bidentate ligand as the active catalyst, which maintained high activity (= TOF) and selectivity even under the high-pressure conditions.^{21,22,38}

Most of the developed strategies for the conversion of FA to H₂ involve amino-functionalized homogeneous or heterogeneous catalysts under atmospheric pressure.^{6,11,39} Heterogeneous catalysts functionalized with amino groups have been reported to exhibit the highest activity (= TOF), whereas the replacement of the amino groups with alkylamino groups or an increased alkyl chain length reduced the catalytic efficiency (= TOF), though the origin of this behavior remain unclear.^{40–42} For homogeneous catalysts, an amino group near the metal center may play an important role in the DFA pathway via protonation of the NH moiety or hydrogen-bonding interactions between the amino groups and water.^{43–45} It has been reported that the introduction of dimethylamino groups to the *para* positions of 2,2'-dipyridylamine afforded a Cp^{*}Ir complex with enhanced catalytic activity (= TOF).⁴⁶ Thus, systematic studies are urgently needed to elucidate the role of amino groups in DFA and develop efficient and robust catalysts.

Herein, we focus on homogeneous Cp^{*}Ir-based catalysts containing amino-functionalized bpy ligands for DFA. We investigate the influence of substituents and their positions on the catalytic performance for producing high-pressure H₂ without any base. Furthermore, a reaction mechanism is proposed based on NMR analyses and kinetic isotope effect (KIE) measurements.

RESULTS AND DISCUSSION

The Ir complexes containing amino-functionalized ligands (**1b**, **1c**, **1d**, and **2b** in Figure 2) were prepared via the reaction of Cp^{*}Ir aqua complex ([Cp^{*}Ir(H₂O)₃]SO₄) with the corre-

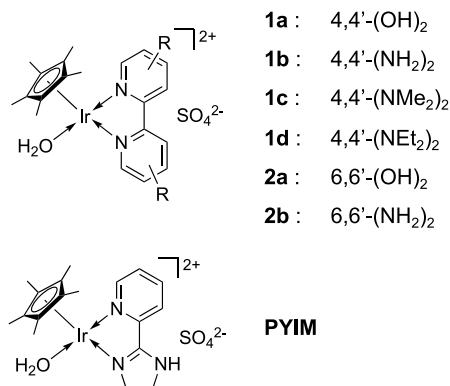


Figure 2. Ir complexes for DFA.

sponding bpy derivatives in water according to a previously reported method.⁴⁷ The resulting complexes were characterized using ¹H NMR and ¹³C NMR spectroscopy (Figures S2–S6). For **1b**, ¹H NMR and ¹³C NMR analysis in D₂O revealed a broad peak corresponding to bpy derived from the classical bifurcated hydrogen bonds between the NH and 5-CH of pyridine⁴⁸ and water (Figure S2), which was in contrast to the other complexes (**1a**, **1c**, **1d** and **2a**), (Figures S3–S6). This peak became sharp and more intense as the temperature was increased from ambient conditions to 50 °C (Figures S7 and S8), owing to the cleavage of the bifurcated hydrogen bonds. In addition, the electronic properties of **1a** changed significantly with pH owing to the presence of a proton-responsive ligand with hydroxyl groups.³⁰ To investigate the influence of pH on the electronic properties of the catalyst, ¹H NMR spectra and UV–vis absorption spectra of complexes **1b–1d** were measured at various pH values to investigate the influence of pH values (Figures S9 and S10–S15 and Table S1). In terms of the ¹H NMR spectra in D₂O, the chemical shifts of each complex varied from acidic (pD < 2) to basic conditions (pD > 12) as summarized in Table 1. For complex **1a**, the signals corresponding to the 3, 3', 5, 5', 6, and 6' positions of the bpy ligand displayed large upfield shifts in the range of 0.11–0.22 ppm, indicating the deprotonation of the OH group at pH = 4.87 (Table 1, entry 1). In contrast, the corresponding signals of complexes **1b–1d** showed small

Table 1. pK_a Values and ¹H NMR Chemical Shifts for the bpy Ligands in the Ir Complexes^a

entry	complex	pK _a	Δppm ^b			
			3,3'-position	4,4'-position	5,5'-position	6,6'-position
1	1a	4.87 ± 0.14 ^c 9.14 ± 0.18	0.22	–	0.17	0.11
2	1b	7.63 ± 0.11	0.04	–	0.02	0.04
3	1c	7.91 ± 0.09	0.02	–	0.01	0.04
4	1d	8.01 ± 0.11	0.01	–	0.01	0.04
5	2a^d	4.7 10.6	0.86	0.59	0.80	–
6	2b	7.39 ± 0.16 9.65 ± 0.10	1.03	1.00	1.02	–

^aDetermined from UV–vis absorption spectra. ^bDetermined from ¹H NMR spectra, where Δppm denotes the change in the chemical shift value from acidic (pH < 2) to basic conditions (pH > 12). ^cpH of deprotonation of the hydroxyl groups on the bpy ligand. ^dFrom ref 30.

upfield shifts of only 0.01–0.04 ppm, suggesting the lack of protonation or deprotonation of the amino groups. We further measured the UV–vis absorption spectra of complexes **1a–1d** over the pH range from 2 to 12. No obvious red-shift of the maximum absorption band was observed for complexes **1b–1d** (Figures S11–S14), which was in contrast to the case of complex **1a** with hydroxyl groups on the bpy ligand (Figure S11).³⁰ These results of ¹H NMR spectroscopy and UV–vis absorption results revealed no change in the electronic properties of the amino-functionalized complexes (**1b–1d**) over the examined pH range under the present reaction conditions.³⁰ The pK_a values of the aqua ligands of **1a–1d** were determined via UV–vis absorbance spectroscopy (Table 1 and Experimental Section in the SI). Deprotonation of the aqua ligands of the amino-functionalized complexes (**1b–1d**) was observed at pH values ranging from 7.63 to 8.01, which are lower than the pH value of 9.2 observed for the hydroxyl-functionalized complex (**1a**). Among the complexes **1b–1d**, pK_a increased upon replacement of the amino groups (**1b**) on the bpy ligand with the dimethylamino groups (**1c**) and remained similar for diethylamino groups (**1d**). Deprotonation of the hydroxyl groups of complex **1a** was observed at pH = 4.87, whereas no protonation or deprotonation of the amino groups occurred for complexes **1b–1d**, as no spectral change was detected over the pH range from 2 to 8.

Initially, we conducted the DFA in water under atmospheric pressure using the Ir-complexes (Table 2). The complex

Table 2. DFA with the Ir Complexes^a

entry	complex	complex conc. /mM	initial FA conc. /M	initial TOF ^b /h ⁻¹	reaction time /h	residual FA conc. /M
1 ^c	1a	0.02	1	1900 ^c	156	0
2	1b	0.02	1	10100	6.8	0
3	1c	0.02	1	12700	5.9	0
4	1d	0.02	1	12700	5.9	0
5 ^c	2a	0.02	1	2200 ^c	123	0
6	2b	0.02	1	17	10 ^d	0.9 ^d
7	2b	1.1	1	24	72	0
8	1c	0.02	3	16200	9.7	0
9 ^c	1c	0.02	3	25000	8.3	0.52
10 ^{e,f}	1c	0.01	3	115500	13	0.53

^aReaction conditions: 60 °C, pressure = 0.1 MPa, catalyst amount = 2–4 μmol. ^bAverage value of two measurements conducted during the initial 10–20 min. The errors for all initial TOFs were within ±5%. ^cThe TOF values obtained in this work; for reference, TOF values of 2400 and 2200 were previously reported for 0.2 mM **1a** and **2a**, respectively.^{12,31} ^dThe gas generation rate analysis was stopped after 10 h. ^eAddition of 15 mol % of NaOH. ^fTemperature = 80 °C.

containing amino groups on the bpy ligand at the *para* positions (**1b**, entry 2 in Table 2) effectively catalyzed DFA compared with the complex containing hydroxyl groups at the same positions (**1a**, entry 1 in Table 2). The incorporation of dimethylamino (**1c**) or diethylamino (**1d**) groups into the bpy ligand slightly enhanced the catalytic activity (= TOF). Based on Hammett plots, recent studies have reported positive effects on DFA after the introduction of electron-donating substituents into the bpy ligand.^{12,31,49} Thus, we correlated the Hammett constants (σ_p⁺)⁵⁰ of the studied electron-donating substituents at the *para* positions of bpy and the catalytic performance (TOF) of the corresponding complexes (Figure 3). A slope of −2.01 was calculated from the Hammett plot of

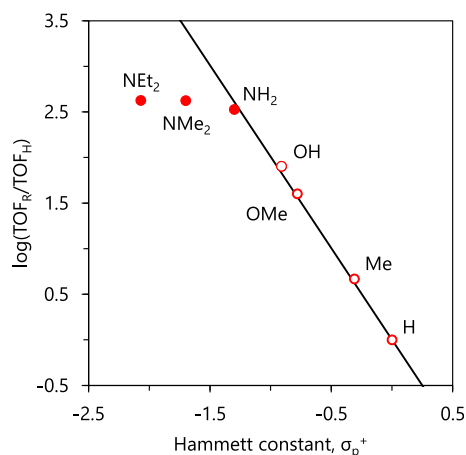


Figure 3. Hammett plot for the rate of DFA (= TOF) catalyzed by the Ir complexes (Cp^*Ir) containing various substituents at the *para* position of the bpy ligand for various catalyst concentrations in 1 M FA solution. The TOF_R denotes the TOFs for the Cp^*Ir catalysts with bpy ligands bearing OH, OMe, Me, and NR_2 ($R = \text{H, Me, Et}$; cat. conc. = 0.02 mM) groups at the *para* positions. TOF_H denotes the TOF for the Cp^*Ir catalyst with bpy ligand ($R = \text{H}$). The TOF values for the Cp^*Ir catalysts with OH (cat. conc. = 0.2 mM), OMe (cat. conc. = 0.2 mM), Me (cat. conc. = 2 mM), and H (cat. conc. = 2 mM) groups were taken from the literature.¹² The Hammett constants were also taken from the literature.⁵⁰ The line was calculated using the Hammett equation.

the $-\text{NH}_2$, $-\text{OH}$, $-\text{OMe}$, Me, and H groups. An obvious relationship was observed between the catalytic activity (= TOF) and the electron-donating ability of the substituents, although no such effect was observed for the dimethylamino (**1c**) and the diethylamino (**1d**) groups where the electron-donating ability increased with increasing alkyl chain length on the amino groups. Note that the deviation of Hammett constants (σ_p^+) from the reference data may be attributable to the changes in the resonance effects between the pyridine moieties and alkylamino chains.⁵⁰ Notably, the Ir complex with the bpy ligand containing *para*-amino groups (**1b**) exhibited a higher TOF compared with that containing *ortho*-amino groups (**2b**).⁵¹ During the ^1H NMR analysis of **2b** in D_2O , the peaks corresponding to the bpy ligand with *ortho*-amino groups remained unchanged even after the addition of excess amount of NaOD (Figure S10(c)), whereas new peaks attributed to the complex containing protonated *ortho*-amino groups appeared after the addition of excess D_2SO_4 (Figure S10(b)). This result implies that under acidic conditions, protonation of the amino groups of **2b** occurred to form $-\text{NH}_3^+$, which then acted as an electron-withdrawing group, thereby accounting for the reduced TOF.

The conversion of FA to H_2 was also accelerated by the addition of base as well as by higher temperatures (entries 9 and 10 in Table 2). For instance, the TOF increased by 1.5-fold upon addition of 15 mol % NaOH into the FA solution and finally reached 115500 h^{-1} on half-concentration of catalyst. Despite this enhanced reaction rate, the remaining FA solution (entries 9 and 10 in Table 2) was converted to formate (HCO_2Na), which is inert as a substrate for H_2 production. Kinetic studies of DFA were conducted at atmospheric pressure. For complexes **1b–1d**, the initial rate of DFA increased with increasing FA concentration up to 3 M and thereafter decreased (Figure S16). The DFA reaction barely proceeded at a high concentration of FA (20 M), and

the addition of water promoted the reaction (Figure S17). During the reaction in the presence of water, FA was completely decomposed into gaseous H_2 and CO_2 and a final TON of 909000 was reached. To confirm the effect of water, DFA was conducted in both water and in a water/1,4-dioxane mixture, where 1,4-dioxane is an aprotic solvent that is miscible with water in any ratio (Table S2). The water concentration appeared to exert a positive influence on the reaction rate, which indicates that the complexes are stable even at high concentrations of FA in water. For complexes **1b–1d**, the catalytic activity (= TOF) reached a maximum value at $\text{pH} = 3.0 \pm 0.1$ and $\text{pH} = 2.5$ in 0.1 and 3 M FA solution, respectively (Figure 4 and Figure S18). The shift of the pH

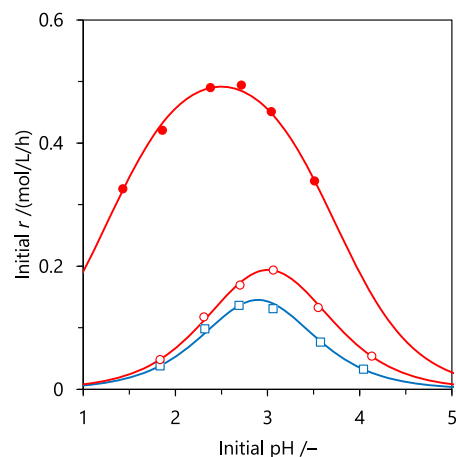
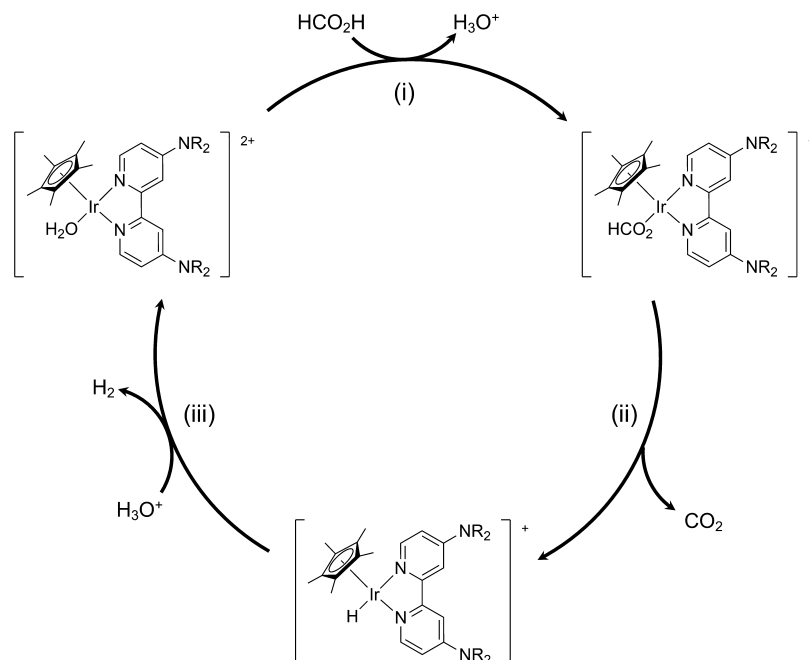
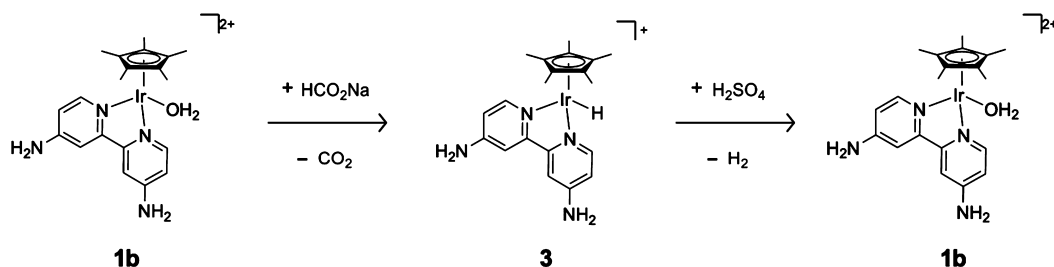


Figure 4. pH dependence of the rate of DFA using Ir complexes (0.02 mM) and various FA concentrations at 60°C : \square , **1b** in 0.1 M FA; \circ , **1c** in 0.1 M FA; \bullet , **1c** in 3 M FA. The pH of the solutions were adjusted by the addition of either NaOH or H_2SO_4 .

corresponding to the highest catalytic activity (= TOF) with increasing FA concentration suggests that the reaction rate can be expressed as a function of the formate and proton concentrations.²⁸ A nominal effect on the rate of FA dehydrogenation was observed in the presence of various bases (OH^- , HCO_3^- , CO_3^{2-} , NEt_3) and Lewis acids (Li^+ , Na^+ , K^+ , Ca^{2+}) (Table S3). Furthermore, a log–log plot of the DFA rate versus the initial complex concentration indicated a first-order reaction with respect to the catalyst concentration (Figure S19). The calculated activation energies (E_a) obtained from the Arrhenius plots were similar for complexes **1b** and **1c** (81.4–82.3 kJ/mol, Figure S20) and were in good agreement with those in previous reports.^{30,31,51}

NMR analyses and KIE measurements were performed to elucidate the mechanism of DFA under the present reaction conditions. On the basis of the experimental results, we proposed the reaction pathway shown in Scheme 1. DFA is considered to proceed via (i) generation of the formate intermediate, (ii) subsequent release of CO_2 via β -hydride elimination to produce a hydride intermediate, and, finally, (iii) generation of H_2 from the hydride intermediate.^{28,31,37} Although GC analysis confirmed the generation of H_2 from the stoichiometric reaction between complex **1b** and sodium formate after the addition of sulfuric acid (Scheme 2 and Figure S21), formation of the hydride intermediate (**3**) remained undetected by ^1H NMR owing to its short lifetime and the rapid H/D exchange between the hydride complex and D_2O .³¹ Hence, to confirm the formation of the hydride

Scheme 1. Proposed Reaction Mechanism for the Dehydrogenation of Formic Acid Using the Ir Complexes

Scheme 2. Stoichiometric Reaction between **1b** and Sodium Formate Followed by the H₂ Release upon Addition of Sulfuric Acid

intermediate of **1b**, the reaction between **1b** and sodium formate was conducted followed by anion metathesis with NaPF₆, which precipitated the hydride complex out of solution and allowed its NMR spectrum to be recorded in the aprotic solvent, DMSO-*d*₆ (**3**, Experimental Section and Figure S22). In contrast, the reaction of complex **2b** with sodium formate generated the hydride intermediate, as demonstrated by the NMR spectroscopy (Figure S23 (b) and (c)), and the GC analysis confirmed the release of H₂ upon the addition of sulfuric acid to the hydride intermediate (Figure S23 (c) and (d)). These NMR and GC results support our proposed mechanism. The NMR analysis also confirmed that the lifetime of the hydride intermediate from **2b** was longer than that from **1b**, which could be correlated with the TOFs of the DFA reactions in the presence of the corresponding catalysts (entries 2 and 6 in Table 2). Furthermore, KIE measurements were conducted to study the rate-determining step of DFA using **1b** through the isotopic substitution of the C–H and O–H groups of FA. Table 3 summarizes the observed reaction rates for the four labeled FA isotopologues (HCO₂H, HCO₂D (HCO₂H + D₂O), DCO₂H, and DCO₂D). Comparison of the KIE values (ratio of the reaction rate constant for the labeled molecule to that for the unlabeled molecule) revealed that deuteration at the carbon atom ($k_{(\text{DCO}_2\text{H})}/k_{(\text{HCO}_2\text{H})} = 2.9$) had a greater effect on DFA than deuteration at the oxygen atom

Table 3. Kinetic Isotope Effect in DFA using **1b**^a

entry	substrate	solvent	TOF ^b /h ⁻¹	KIE ^c
1	HCO ₂ H	H ₂ O	7700 ± 200	–
2	HCO ₂ H	D ₂ O	5400 ± 300	1.42 ± 0.04
3	DCO ₂ D	H ₂ O	2700 ± 100	2.85 ± 0.03
4	DCO ₂ D	D ₂ O	2900 ± 100	2.65 ± 0.02

^aReaction conditions: temperature = 60 °C, pressure = 0.1 MPa, catalyst amount = 2 μmol, initial FA solution = 1 mol/L, 20 mL. ^bAverage value over the first 30 min. ^cKIE is defined as the TOF ratio of entry 1 to entry *n*, where *n* is set to 2, 3, or 4.

($k_{(\text{HCO}_2\text{D})}/k_{(\text{HCO}_2\text{H})} = 1.4$). Thus, the β-elimination step is the rate-determining step for this reaction, whereas the KIE value of $k_{(\text{DCO}_2\text{D})}/k_{(\text{HCO}_2\text{H})} = 2.7$ was almost the same as the value of $k_{(\text{DCO}_2\text{H})}/k_{(\text{HCO}_2\text{H})} = 2.9$ owing to the nominal influence of the O–H group of FA on the reaction. This result is consistent with the short lifetime of the iridium hydride intermediate, which produces H₂ more rapidly than CO₂.

The influence of the temperature on the generation of high-pressure H₂ using complexes (**1b**–**1d**) was also examined. At 50 °C, >20 MPa of high-pressure gas was generated from 7 M FA solution in the presence of **1b**. This experiment could be repeated at least three times without showing in the generation rate (Figure S24). Furthermore, at 80 °C complex **1c** produced a very high gas pressure of 157 MPa within 4 h from the 21 M

of FA solution (Figure 5). The resulting high-pressure gas was composed of H₂ and CO₂ in the same molar ratio, whereas no

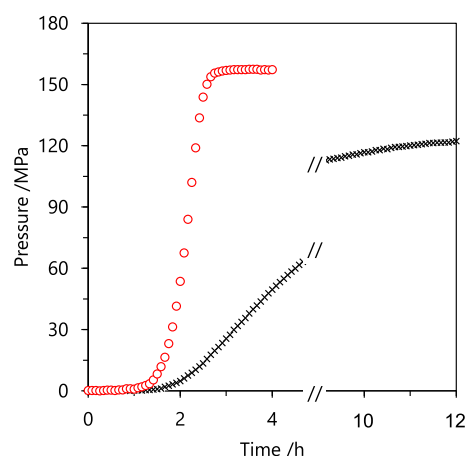


Figure 5. Time course of the generated pressure by the DFA at 80 °C in highly concentrated FA solution using the Ir complexes (2 mM): ×, **1a** in 20 M FA; ○, **1c** in 21 M FA.

CO (<6 vol ppm) was detected by GC analysis (Figure S25). Under similar conditions, a maximum gas pressure of 123 MPa was obtained using **1a** owing to catalyst deactivation.²² Furthermore, we compared the reaction rates for complexes **1a**, **1b**, **1c**, and **1d** and an Ir complex bearing 2-(2'-pyridyl)imidazoline (PYIM) to reach a pressure of 40 MPa (Table 4), as PYIM was previously reported to generated the

Table 4. High-Pressure DFA using the Ir Complexes^a

entry	complex	complex conc. /mM	initial TOF ^b /h ⁻¹	reaction time /h	residual FA conc. /M
1	1a	0.4	1900	14.0	0.55
2	1b	0.2	8500	5.2	0.42
3	1c	0.2	14600	3.7	0.40
4	1d	0.2	16900	2.2	0.37
5	PYIM	0.2	6500	18.2	9.99
6	PYIM	0.4	9000	2.4	0.40

^aReaction conditions: temperature = 80 °C, pressure = 40 MPa, catalyst amount = 8 or 16 μmol, initial FA solution = 16 M, 40 mL.
^bAverage value over the initial 10–30 min.

highest pressure of 153 MPa from DFA.²² The highest TOF (16900 h⁻¹) was obtained in 16 M FA solution using **1d** at 80 °C. The flow rate of the high-pressure gas (H₂ and CO₂) generated by DFA increased gradually with time during the reaction (Figure S26) and might be correlated with the FA concentration. Under these conditions, the equilibrium concentration of FA was estimated as 0.37 ± 0.01 M. This high-pressure reaction was performed using the low concentrations of **1b**, **1c**, and **1d**, and a high concentration of PYIM. Based on the residual FA concentration after the reactions, the complexes were arranged in descending order of catalytic stability (**1d** ≅ **1c** ≅ **1b** > PYIM > **1a**).

To assess the long-term reactivity, the Ir complexes were subjected to continuous-flow measurements at 50 °C (Table 5). We first studied the decomposition of FA using **1a** and **1b** at atmospheric pressure by adding neat FA to the solution at a constant rate via a liquid pump. In the case of **1a**, FA was continuously and selectively decomposed into H₂ and CO₂ gases over 200 h without any detection of CO (detection limit

Table 5. Continuous DFA using the Ir Complexes^a

entry	complex	pressure /MPa	stability ^b /h	CO /vol. ppm	TON _{80%} ^c
1	1a	0.1	60	n.d. ^d	66500
2	1a	20	10	n.d.	5829
3	1b	0.1	120	n.d.	402000
4	1b	20	60	n.d.	72400
5	1c	20	40	n.d.	50300
6	1d	20	30	n.d.	39100
7 ^e	PYIM	20	30	n.d.	45800

^aReaction conditions: temperature = 50 °C, catalyst amount = 16 μmol, initial FA solution = 5 M, 40 mL. FA was added at a rate of 0.6 mL/h over 10 h using a plunger pump and then stopped for several hours. This process was repeated several times. ^bTime elapsed from the beginning until a decrease in the gas generation rate. ^cCalculated value when the gas flow rate had decreased by 80% of the initial rate. ^dBelow the detection limit (<6 vol. ppm). ^eData taken from the literature.²²

< 6 vol ppm, Figure S28). From 20 to 30 h of FA addition, the gas flow rate was measured as 0.62 L/h (13 mmol-H₂/h), and the corresponding FA flow rate was 0.4 mL/h (11 mmol/h). However, the gas flow rate gradually decreased over time during FA addition. When the gas flow rate had decreased by 80% from the initial rate, a TON of 66500 (TON_{80%}, Table 5, entry 1) was calculated from the volume of H₂. In the case of **1b**, the average gas flow rate from 10 to 20 h of FA addition was 0.80 L/h (16 mmol-H₂/h). When the gas flow rate had decreased by 80% and 50% from the initial rate, TONs were 402000 (TON_{80%}, Table 5, entry 2) and 515000 (TON_{50%}), respectively. The TON_{80%} for complex **1b** (402000) was therefore 6-fold larger than that for **1a** (TON_{80%} = 66500, Figures S29 and S30). Owing to the residual FA in the solution, the gas generation continued even after the addition of FA had been stopped. Finally, when the FA decomposition had reached completion, a TON of 974000 was calculated from the total gas volume of H₂.

Next, the catalytic stability of the complexes was studied during continuous DFA at 20 MPa and 50 °C, and the generated gas flow rate was measured. Complex **1a** became deactivated after the system reached 20 MPa (entry 2 in Table 5) owing to the formation of polymeric compounds with the generated H₂ which indicated limited stability under high pressure.²¹ As determined using the stop and flow method, complex **1b** was able to generate the high-pressure gas with a constant pressure of 20 MPa over six cycles of FA addition, although the pressure gradually decreased thereafter (Figure 6). Complex **1b** retained its stability for 60 h under high pressure and afforded a TON_{80%} value of 72400 (entry 4 in Table 5). Complexes **1c** and **1d** also allowed a constant flow rate of the generated gas to be maintained for six and three cycles of FA addition, respectively, and the TON_{80%} for **1c** (50300, Figure S30) was greater than that for **1d** (39100, Figure S31). In addition, we also observed that the resonance associated with the amine and pyridine groups, which increases with increasing electron density of the pyridine nitrogen atom, had less effect on the stability than on the activity of the catalyst. As mentioned above, we observed the highest pressure of 153 MPa during DFA using the Ir-PYIM catalyst, although the PYIM ligand lost its stability after 30 h at 20 MPa with a TON_{80%} of 45800. Thus, the incorporation of amino groups at the *para* positions of pyridine improves the catalytic activity (= TOF) and stability (= TON_{80%}) during high-pressure DFA. It should be noted that during the continuous-flow measure-

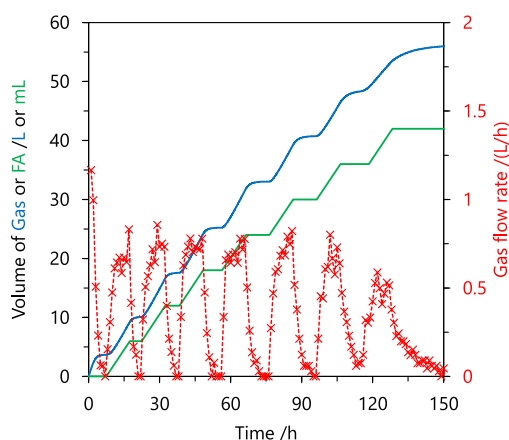


Figure 6. Continuous DFA using **1b** (16 μmol) at 50 $^{\circ}\text{C}$ and 20 MPa. Blue line, generated gas volume; green line, added FA volume; \times , flow rate of generated gas. Time elapsed after reaching the pressure of 20 MPa. FA was added at high-pressure at a rate of 0.6 mL/h over 10 h, and the FA addition was repeated seven times.

ments, a decrease in the catalytic activity resulted in an increase in the residual concentration of FA, which led to a change in the reaction rate as a function of FA concentration. To eliminate the influence of residual reactant, neat FA was continuously added to the solution for 10 h after the gas generation had stopped, and each experiment was repeated several times.

CONCLUSIONS

We have synthesized a series of Cp^*Ir complexes containing bpy ligands bearing amino or alkylamino groups to investigate the influence of the ligand on DFA in water under base-free conditions. The Ir complexes containing amino groups at the *para* positions of the bpy ligand exhibited high activity even at high pressures compared with those containing hydroxyl groups or *ortho*-amino groups on the bpy ligand. Furthermore, despite the enhanced catalytic activity obtained after replacing the amino groups by alkylamino groups, the stability of the Ir complexes decreased. A Hammett plot demonstrated that electron donation from the substituents at the *para* positions of the bpy ligand increased the rate of DFA. In addition, NMR analyses revealed faster dehydrogenation from the hydride intermediate in the case of the IrCp^* catalyst having a *para*-amino-substituted bpy ligand. The results of this work illustrate the electronic effects of these functionalized ligands on the activity and stability during the generation of high-pressure H_2 from FA, and we anticipate that the strategy outlined herein will help guide future catalyst development involving the introduction of functional groups into these ligands.

ASSOCIATED CONTENT

Supporting Information

The Supporting Information is available free of charge at <https://pubs.acs.org/doi/10.1021/acs.inorgchem.9b01624>.

Experimental section, including general procedures, synthesis of the complexes, and calculations of the $\text{p}K_{\text{a}}$, TOF, and TON values; ^1H NMR, ^{13}C NMR, and UV–vis absorption spectra of the complexes; DFA reaction rate at various concentrations of FA, water, bases, and the complexes; pH and temperature dependence of the reaction rate; the ^1H NMR and KIE studies of the

reaction mechanism; high-pressure gas generation by DFA; GC chromatogram of the gaseous products; and continuous DFA at atmospheric and high pressures (PDF)

AUTHOR INFORMATION

Corresponding Author

Hajime Kawanami – Research Institute for Chemical Process Technology, Department of Material and Chemistry, National Institute of Advanced Industrial Science and Technology, Sendai, Miyagi 983-8551, Japan; orcid.org/0000-0002-2679-2662; Email: h-kawanami@aist.go.jp; Fax: +81-22-237-5388

Authors

Masayuki Iguchi – Research Institute for Chemical Process Technology, Department of Material and Chemistry, National Institute of Advanced Industrial Science and Technology, Sendai, Miyagi 983-8551, Japan

Yuichiro Himeda – Research Institute of Energy Frontier, Department of Energy and Environment, National Institute of Advanced Industrial Science and Technology, Tsukuba, Ibaraki 305-8565, Japan; orcid.org/0000-0002-9869-5554

Complete contact information is available at:

<https://pubs.acs.org/10.1021/acs.inorgchem.9b01624>

Notes

CAUTION! Although hydrogen gas has no reactivity or toxicity hazards, it can ignite upon exposure to air. Hence, the generated gas from DFA (50% of H_2 and 50% of CO_2) should be diluted with a large quantity of N_2 gas to reduce its H_2 content to less than 4% before releasing it to the air. Therefore, all experiments must be conducted inside a fume-hood with appropriate safety precautions. The authors declare no competing financial interest.

ACKNOWLEDGMENTS

M.I. and H.K. thank Dr. Maya Chatterjee (National Institute of Advanced Industrial Science and Technology in Sendai) for help in preparing and correcting the manuscript through discussions. The authors thank Dr. Alexander Pyatenko (National Institute of Advanced Industrial Science and Technology in Tsukuba) for performing the elemental analysis. The authors would like to acknowledge the financial support of the Japan Science and Technology Agency (JST), CREST (JPMJCR1342), and the International Joint Research Program for Innovative Energy Technology of the Ministry of Economy, Trade, and Industry (METI) of Japan.

REFERENCES

- (1) Orimo, S.-i.; Nakamori, Y.; Eliseo, J. R.; Zuttel, A.; Jensen, C. M. Complex Hydrides for Hydrogen Storage. *Chem. Rev.* **2007**, *107*, 4111–4132.
- (2) Preuster, P.; Alekseev, A.; Wasserscheid, P. Hydrogen Storage Technologies for Future Energy Systems. *Annu. Rev. Chem. Biomol. Eng.* **2017**, *8*, 445–471.
- (3) Preuster, P.; Papp, C.; Wasserscheid, P. Liquid Organic Hydrogen Carriers (LOHCs): Toward a Hydrogen-free Hydrogen Economy. *Acc. Chem. Res.* **2017**, *50* (1), 74–85.
- (4) Felderhoff, M.; Weidenthaler, C.; von Helmolt, R.; Eberle, U. Hydrogen storage: the remaining scientific and technological challenges. *Phys. Chem. Chem. Phys.* **2007**, *9* (21), 2643–2653.
- (5) Jensen, J. O.; Vestbø, A. P.; Li, Q.; Bjerrum, N. J. The energy efficiency of onboard hydrogen storage. *J. Alloys Compd.* **2007**, *446–447*, 723–728.

- (6) Mellmann, D.; Sponholz, P.; Junge, H.; Beller, M. Formic acid as a hydrogen storage material - development of homogeneous catalysts for selective hydrogen release. *Chem. Soc. Rev.* **2016**, *45* (14), 3954–3988.
- (7) Singh, A. K.; Singh, S.; Kumar, A. Hydrogen energy future with formic acid: a renewable chemical hydrogen storage system. *Catal. Sci. Technol.* **2016**, *6*, 12–40.
- (8) Eppinger, J.; Huang, K.-W. Formic Acid as a Hydrogen Energy Carrier. *ACS Energy Letters* **2017**, *2* (1), 188–195.
- (9) Bulushev, D.; Ross, J. R. H. Towards Sustainable Production of Formic Acid from Biomass for Getting Hydrogen and Fuels. *ChemSusChem* **2018**, *11* (5), 821–836.
- (10) Sordakis, K.; Tang, C.; Vogt, L. K.; Junge, H.; Dyson, P. J.; Beller, M.; Laurenczy, G. Homogeneous Catalysis for Sustainable Hydrogen Storage in Formic Acid and Alcohols. *Chem. Rev.* **2018**, *118* (2), 372–433.
- (11) Zhong, H.; Iguchi, M.; Chatterjee, M.; Himeda, Y.; Xu, Q.; Kawanami, H. Formic Acid-Based Liquid Organic Hydrogen Carrier System with Heterogeneous Catalysts. *Advanced Sustainable Systems* **2018**, *2* (2), 1700161.
- (12) Himeda, Y. Highly efficient hydrogen evolution by decomposition of formic acid using an iridium catalyst with 4,4'-dihydroxy-2,2'-bipyridine. *Green Chem.* **2009**, *11* (12), 2018–2022.
- (13) Hull, J. F.; Himeda, Y.; Wang, W.-H.; Hashiguchi, B.; Periana, R.; Szalda, D. J.; Muckerman, J. T.; Fujita, E. Reversible hydrogen storage using CO₂ and a proton-switchable iridium catalyst in aqueous media under mild temperatures and pressures. *Nat. Chem.* **2012**, *4* (5), 383–388.
- (14) Onishi, N.; Xu, S.; Manaka, Y.; Suna, Y.; Wang, W.-H.; Muckerman, J. T.; Fujita, E.; Himeda, Y. CO₂ Hydrogenation Catalyzed by Iridium Complexes with a Proton-Responsive Ligand. *Inorg. Chem.* **2015**, *54* (11), 5114–5123.
- (15) Suna, Y.; Himeda, Y.; Fujita, E.; Muckerman, J. T.; Ertem, M. Z. Iridium Complexes with Proton-Responsive Azole-Type Ligands as Effective Catalysts for CO₂ Hydrogenation. *ChemSusChem* **2017**, *10* (22), 4535–4543.
- (16) Niermann, M.; Beckendorff, A.; Kaltschmitt, M.; Bonhoff, K. Liquid Organic Hydrogen Carrier (LOHC) - Assessment based on chemical and economic properties. *Int. J. Hydrogen Energy* **2019**, *44* (13), 6631–6654.
- (17) Wang, W.-H.; Himeda, Y.; Muckerman, J. T.; Manbeck, G. F.; Fujita, E. CO₂ Hydrogenation to Formate and Methanol as an Alternative to Photo- and Electrochemical CO₂ Reduction. *Chem. Rev.* **2015**, *115* (23), 12936–12973.
- (18) Celaje, J. J. A.; Lu, Z.; Kedzie, E. A.; Terrile, N. J.; Lo, J. N.; Williams, T. J. A prolific catalyst for dehydrogenation of neat formic acid. *Nat. Commun.* **2016**, *7*, 11308.
- (19) Matubayasi, N.; Nakahara, M. Hydrothermal reactions of formaldehyde and formic acid: Free-energy analysis of equilibrium. *J. Chem. Phys.* **2005**, *122* (7), 074509.
- (20) Müller, K.; Brooks, K.; Autrey, T. Hydrogen Storage in Formic Acid: A Comparison of Process Options. *Energy Fuels* **2017**, *31* (11), 12603–12611.
- (21) Iguchi, M.; Himeda, Y.; Manaka, Y.; Matsuoka, K.; Kawanami, H. Simple Continuous High-Pressure Hydrogen Production and Separation System from Formic Acid under Mild Temperatures. *ChemCatChem* **2016**, *8* (5), 886–890.
- (22) Iguchi, M.; Chatterjee, M.; Onishi, N.; Himeda, Y.; Kawanami, H. Sequential hydrogen production system from formic acid and H₂/CO₂ separation under high-pressure conditions. *Sustainable Energy & Fuels* **2018**, *2* (8), 1719–1725.
- (23) Fellay, C.; Dyson, P. J.; Laurenczy, G. A Viable Hydrogen-Storage System Based On Selective Formic Acid Decomposition with a Ruthenium Catalyst. *Angew. Chem., Int. Ed.* **2008**, *47* (21), 3966–3968.
- (24) Guan, C.; Zhang, D.-D.; Pan, Y.; Iguchi, M.; Ajitha, M. J.; Hu, J.; Li, H.; Yao, C.; Huang, M.-H.; Min, S.; Zheng, J.; Himeda, Y.; Kawanami, H.; Huang, K.-W. Dehydrogenation of Formic Acid Catalyzed by a Ruthenium Complex with an N,N'-Diimine Ligand. *Inorg. Chem.* **2017**, *56* (1), 438–445.
- (25) Papp, G.; Olveti, G.; Horvath, H.; Katho, A.; Joó, F. Highly efficient dehydrogenation of formic acid in aqueous solution catalysed by an easily available water-soluble iridium(III) dihydride. *Dalton Transactions* **2016**, *45* (37), 14516–14519.
- (26) Zhong, H.; Iguchi, M.; Song, F.-Z.; Chatterjee, M.; Ishizaka, T.; Nagao, I.; Xu, Q.; Kawanami, H. Automatic high-pressure hydrogen generation from formic acid in the presence of nano-Pd heterogeneous catalysts at mild temperatures. *Sustainable Energy & Fuels* **2017**, *1* (5), 1049–1055.
- (27) Iguchi, M.; Zhong, H.; Himeda, Y.; Kawanami, H. Effect of the Ortho-Hydroxyl Groups on Bipyridine Ligand of Iridium Complexes for High-Pressure Gas Generation from Catalytic Decomposition of Formic Acid. *Chem. - Eur. J.* **2017**, *23* (70), 17788–17793.
- (28) Iguchi, M.; Zhong, H.; Himeda, Y.; Kawanami, H. Kinetic Studies on Formic Acid Dehydrogenation Catalyzed by an Iridium Complex towards Insights into the Catalytic Mechanism of High-Pressure Hydrogen Gas Production. *Chem. - Eur. J.* **2017**, *23* (67), 17017–17021.
- (29) Anderson, N. H.; Boncella, J. M.; Tondreau, A. M. Reactivity of Silanes with (tBuPONOP)Ruthenium Dichloride: Facile Synthesis of Chloro-Silyl Ruthenium Compounds and Formic Acid Decomposition. *Chem. - Eur. J.* **2017**, *23* (55), 13617–13622.
- (30) Suna, Y.; Ertem, M. Z.; Wang, W.-H.; Kambayashi, H.; Manaka, Y.; Muckerman, J. T.; Fujita, E.; Himeda, Y. Positional Effects of Hydroxy Groups on Catalytic Activity of Proton-Responsive Half-Sandwich Cp*Ir(III) Complexes. *Organometallics* **2014**, *33* (22), 6519–6530.
- (31) Wang, W.-H.; Xu, S.; Manaka, Y.; Suna, Y.; Kambayashi, H.; Muckerman, J. T.; Fujita, E.; Himeda, Y. Formic Acid Dehydrogenation with Bioinspired Iridium Complexes: A Kinetic Isotope Effect Study and Mechanistic Insight. *ChemSusChem* **2014**, *7* (7), 1976–1983.
- (32) Wang, W.-H.; Ertem, M. Z.; Xu, S.; Onishi, N.; Manaka, Y.; Suna, Y.; Kambayashi, H.; Muckerman, J. T.; Fujita, E.; Himeda, Y. Highly Robust Hydrogen Generation by Bioinspired Ir Complexes for Dehydrogenation of Formic Acid in Water: Experimental and Theoretical Mechanistic Investigations at Different pH. *ACS Catal.* **2015**, *5* (9), 5496–5504.
- (33) Onishi, N.; Ertem, M. Z.; Xu, S.; Tsurusaki, A.; Manaka, Y.; Muckerman, J. T.; Fujita, E.; Himeda, Y. Direction to practical production of hydrogen by formic acid dehydrogenation with Cp*Ir complexes bearing imidazoline ligands. *Catal. Sci. Technol.* **2016**, *6*, 988–992.
- (34) Wang, L.; Onishi, N.; Murata, K.; Hirose, T.; Muckerman, J. T.; Fujita, E.; Himeda, Y. Efficient Hydrogen Storage and Production Using a Catalyst with an Imidazoline-Based, Proton-Responsive Ligand. *ChemSusChem* **2017**, *10* (6), 1071–1075.
- (35) Kanega, R.; Onishi, N.; Wang, L.; Murata, K.; Muckerman, J. T.; Fujita, E.; Himeda, Y. Picolinamide-Based Iridium Catalysts for Dehydrogenation of Formic Acid in Water: Effect of Amide N Substituent on Activity and Stability. *Chem. - Eur. J.* **2018**, *24* (69), 18389–18392.
- (36) Onishi, N.; Kanega, R.; Fujita, E.; Himeda, Y. Carbon Dioxide Hydrogenation and Formic Acid Dehydrogenation Catalyzed by Iridium Complexes Bearing Pyridyl-pyrazole Ligands: Effect of an Electron-donating Substituent on the Pyrazole Ring on the Catalytic Activity and Durability. *Adv. Synth. Catal.* **2019**, *361* (2), 289–296.
- (37) Ertem, M. Z.; Himeda, Y.; Fujita, E.; Muckerman, J. T. Interconversion of Formic Acid and Carbon Dioxide by Proton-Responsive, Half-Sandwich Cp*Ir^{III} Complexes: A Computational Mechanistic Investigation. *ACS Catal.* **2016**, *6* (2), 600–609.
- (38) Iguchi, M.; Himeda, Y.; Manaka, Y.; Kawanami, H. Development of an Iridium-Based Catalyst for High-Pressure Evolution of Hydrogen from Formic Acid. *ChemSusChem* **2016**, *9* (19), 2749–2753.

(39) Iglesias, M.; Oro, L. A. Mechanistic Considerations on Homogeneously Catalyzed Formic Acid Dehydrogenation. *Eur. J. Inorg. Chem.* **2018**, 2018 (20–21), 2125–2138.

(40) Mori, K.; Masuda, S.; Tanaka, H.; Yoshizawa, K.; Che, M.; Yamashita, H. Phenylamine-functionalized mesoporous silica supported PdAg nanoparticles: a dual heterogeneous catalyst for formic acid/CO₂-mediated chemical hydrogen delivery/storage. *Chem. Commun.* **2017**, 53 (34), 4677–4680.

(41) Song, F.-Z.; Zhu, Q.-L.; Tsumori, N.; Xu, Q. Diamine-Alkalinized Reduced Graphene Oxide: Immobilization of Sub-2 nm Palladium Nanoparticles and Optimization of Catalytic Activity for Dehydrogenation of Formic Acid. *ACS Catal.* **2015**, 5 (9), 5141–5144.

(42) Wang, Z.; Hao, X.; Hu, D.; Li, L.; Song, X.; Zhang, W.; Jia, M. PdAu bimetallic nanoparticles anchored on amine-modified mesoporous ZrSBA-15 for dehydrogenation of formic acid under ambient conditions. *Catal. Sci. Technol.* **2017**, 7 (11), 2213–2220.

(43) Matsunami, A.; Kayaki, Y.; Ikariya, T. Enhanced Hydrogen Generation from Formic Acid by Half-Sandwich Iridium(III) Complexes with Metal/NH Bifunctionality: A Pronounced Switch from Transfer Hydrogenation. *Chem. - Eur. J.* **2015**, 21 (39), 13513–13517.

(44) Iturmendi, A.; Rubio-Pérez, L.; Pérez-Torrente, J. J.; Iglesias, M.; Oro, L. A. Impact of Protic Ligands in the Ir-Catalyzed Dehydrogenation of Formic Acid in Water. *Organometallics* **2018**, 37, 3611.

(45) Cohen, S.; Borin, V.; Schapiro, I.; Musa, S.; De-Botton, S.; Belkova, N. V.; Gelman, D. Ir(III)-PC(sp³)P Bifunctional Catalysts for Production of H₂ by Dehydrogenation of Formic Acid: Experimental and Theoretical Study. *ACS Catal.* **2017**, 7 (12), 8139–8146.

(46) Wang, S.; Huang, H.; Roisnel, T.; Bruneau, C.; Fischmeister, C. Base-free dehydrogenation of aqueous and neat formic acid with Iridium(III)Cp*(dipyridylamine) catalysts. *ChemSusChem* **2019**, 12 (1), 179–184.

(47) Xu, S.; Onishi, N.; Tsurusaki, A.; Manaka, Y.; Wang, W.-H.; Muckerman, J. T.; Fujita, E.; Himeda, Y. Efficient Cp*Ir Catalysts with Imidazoline Ligands for CO₂ Hydrogenation. *Eur. J. Inorg. Chem.* **2015**, 2015 (34), 5591–5594.

(48) Hursthouse, M. B.; Montis, R.; Niitsoo, L.; Sarson, J.; Threlfall, T. L.; Asiri, A. M.; Khan, S. A.; Obaid, A. Y.; Al-Harbi, L. M. Anhydrides and/or hydrates in nitrate, sulphate and phosphate salts of 4-aminopyridine (4-AP) and 3,4-diaminopyridine (3,4-DAP): the role of the water molecules in the hydrates. *CrystEngComm* **2014**, 16 (11), 2205.

(49) Himeda, Y.; Onozawa-Komatsuzaki, N.; Sugihara, H.; Kasuga, K. Recyclable Catalyst for Conversion of Carbon Dioxide into Formate Attributable to an Oxyanion on the Catalyst Ligand. *J. Am. Chem. Soc.* **2005**, 127 (38), 13118–13119.

(50) Hansch, C.; Leo, A.; Taft, R. W. A survey of Hammett substituent constants and resonance and field parameters. *Chem. Rev.* **1991**, 91 (2), 165–195.

(51) Fink, C.; Laurenczy, G. CO₂ as a hydrogen vector - transition metal diamine catalysts for selective HCOOH dehydrogenation. *Dalton Transactions* **2017**, 46 (5), 1670–1676.